Ultrasound modulation of coherent light in a multiple-scattering medium: experimental verification of nonzero average phase carried by light

Mayanglambam Suheshkumar Singh,[1] Rajan Kanhirodan,[1,*] Ram Mohan Vasu,[2] and Debasish Roy[3]

[1]*Department of Physics, Indian Institute of Science, Bangalore 560 012, India*
[2]*Department of Instrumentation and Applied Physics, Indian Institute of Science, Bangalore 560 012, India*
[3]*Department of Civil Engineering, Indian Institute of Science, Bangalore 560 012, India*
[*]*rajan@physics.iisc.ernet.in*

Abstract: We demonstrate the phase fluctuation introduced by oscillation of scattering centers in the focal volume of an ultrasound transducer in an optical tomography experiment has a nonzero mean. The conditions to be met for the above are: (i) the frequency of the ultrasound should be in the vicinity of the most dominant natural frequency of vibration of the ultrasound focal volume, (ii) the corresponding acoustic wavelength should be much larger than ℓ_n^*, a modified transport mean-free-path applicable for phase decorrelation and (iii) the focal volume of the ultrasound transducer should not be larger than $4 - 5$ times $(\ell_n^*)^3$. We demonstrate through simulations that as the ratio of the ultrasound focal volume to $(\ell_n^*)^3$ increases, the average of the phase fluctuation decreases and becomes zero when the focal volume becomes greater than around $4(\ell_n^*)^3$; and through simulations and experiments that as the acoustic frequency increases from $100\ Hz$ to $1\ MHz$, the average phase decreases to zero. Through experiments done in chicken breast we show that the average phase increases from around $110°$ to $130°$ when the background medium is changed from water to glycerol, indicating that the average of the phase fluctuation can be used to sense changes in refractive index deep within tissue.

© 2012 Optical Society of America

OCIS codes: (170.0170) Medical optics and biotechnology; (170.3880) Medical and biological imaging; (110.0110) Imaging systems; (110.6150) Speckle imaging; (110.7170) Ultrasound.

References and links

1. F. A. Marks, H. W. Tomlinson, and G. W. Brooksby, "A comprehensive approach to breast cancer detection using light: photon localization by ultrasound modulation and tissue characterization by spectral discrimination," Proc. SPIE **1888**, 500-510 (1993).
2. L. V. Wang, S. L. Jacques, and X. Zhao, "Continuous wave ultrasonic modulation of scattered laser light to image objects in turbid media," Opt. Lett. **20**(6), 629-631 (1995).
3. S. Sakadzic and L. V. Wang, "Correlation transfer and diffusion of ultrasound-modulated multiply scattered light," Phys. Rev. Lett. **96**, 163902 (2006).
4. S. Sakadzic and L. V. Wang. "Modulation of multiply scattered coherent light by ultrasonic pulses: an analytical model," Phy. Rev. E. **72**, 036620 (2005).

5. M. Kempe, M. Larionov, D. Zaslavsky, and A. Z. Genack, "Acousto-optic tomography with multiply scattered light," J. Opt. Soc. Am. **14**(5), 1151-1158 (1997).
6. R. S. Chandran, D. Roy, R. Kanhirodan, R. M. Vasu, and C. U. Devi, "Ultrasound modulated optical tomography: Young's modulus of the insonified region from measurement of natural frequency of vibration," Opt. Exp. **19**(23), 22837-22850 (2011).
7. T. Durduran, R. Choe, J. P. Culver, L. Zubkov, M. J. Holboke, J. Giammarco, B. Chance, and A. G. Yodh, "Bulk optical properties of healthy female breast tissue," Phys. Med. Biol. **47**, 2847-2861 (2002).
8. C. U. Devi, R. M. Vasu, and A. K. Sood, "Design, fabrication, and characterization of a tissue-equivalent phantom for optical elastography," J. Biomed. Opt. **10**(4), 044020 (2005).
9. W. F. Cheong, S. A. Prahl, and A. J. Welch, "A review of the optical properties of biological tissues," IEEE J. Quant. Elect. **26**(12), 2166-2185 (1990).
10. T. Kamakura, T. Ishiwata, and K. Matsuda, "Model equation for strongly focused finite-amplitude sound beams," J. Acoust. Soc. Am. **107**(6), 3035-3046 (2000).
11. M. Suheshkumar Singh, P. K. Yalavarthy, K. Rajan, and R. M. Vasu, "Assessment of the effect of ultrasound modulation of near infrared light on the quantification of scattering coefficient," Med. Phys. **37**(7), 3744-3751 (2010).
12. L. Wang, S. L. Jacques, and L. Zheng, "MCML-Monte Carlo modeling of light transport in multi-layered tissues," Comput. Meth. Prog. Biomed. **47**(2), 131-146 (1995).
13. S. Leveque-Fort, A. C. Boccara, M. Lebec, and H. Saint-Jalmes, "Ultrasonic tagging of photon paths in scattering media: parallel speckle modulation processing," Opt. Lett. **24**(3), 181-183 (1999).
14. J. Li and L. V. Wang, "Methods for parallel-detection-based ultrasound modulated optical tomography," Appl. Opt. **41**(10), 2079-2084 (2002).
15. K. Creath, "Phase-shifting speckle interferometry," Appl. Opt. **24** (18), 3053-3058 (1985).

1. Introduction

Ultrasound modulated optical tomography (UMOT) combines the advantages of an optical property recovery in a scattering medium with the high resolution available with focused ultrasound (US) [1, 2]. Focused US creates a perturbation in mean position of the scattering centers and refractive index (n) in the focal volume of the focusing US transducer, which is the region of interest (ROI) for imaging. Coherent light picks-up a phase modulation from the ROI which is observed as an intensity modulation in the speckle formed through beating of exiting light. The modulation depth (M), obtained from the speckle intensity or field autocorrelation, is the measurement, from which both the optical (for example, absorption coefficient (μ_a)) and mechanical properties (for example, the shear modulus (G)) pertaining to the ROI are ascertained.

The parent discipline whose extension UMOT is, is diffusing wave spectroscopy (DWS) wherein coherent light is employed to study multiple scattering media undergoing temperature-induced Brownian motion. The measurement is a correlation function (field- or intensity autocorrelation; $g_1(\tau)$ or $g_2(\tau)$ respectively) whose decay is used to quantitatively measure the mean complex modulus of elasticity of the medium. In UMOT we add a local, deterministic sinusoidal perturbation to the stochastically driven multiple scattering medium at the focal region of the US transducer. This perturbation gives rise to a sinusoidal modulation on the correlation fluctuation. The speckle modulation mentioned earlier is a measure of the modulation in $g_1(\tau)$ whose depth M is related to μ_a and G of the US focal volume.

A general assumption under which quantitative expressions connecting $g_1(\tau)$ to the properties of the object is derived both in DWS and UMOT is that the optical wavelength $\lambda_\circ$ is very small compared to the scattering mean-free-path (ℓ_s) [3, 4], which is the so-called weak scattering condition. This would imply that correlation of light reaching the detector along different paths is negligibly small and only light traveling the same path contributes to $g_1(\tau)$. Another assumption in regard to UMOT is that the phase increments $(\Delta\phi)$ introduced by US forcing of scattering centers within the ROI are uncorrelated. This is true when $\lambda_a << \ell^*$ where λ_a is the acoustic wavelength and ℓ^* is the transport mean-free-path of light in the medium. In addition, one also assumes that the random process associated with the overall phase fluctuation picked-

up within the object is wide-sense stationary which is true when the object dimensions are large compared to λ_a.

The above assumptions, particularly, the uncorrelatedness of $\Delta\phi$ within the ROI makes the phase measured in the $g_1(\tau)$ modulation (i.e., the speckle interference term) a random variable with zero mean and therefore, carrying no useful information. On the other hand, when the acoustic excitation is of low frequency (say $< 1\ kHz$) the assumption $\lambda_a << \ell^*$ is violated, and more importantly when the acoustic excitation is in the neighborhood of one of the dominant natural frequencies of vibration of the insonified US focal region, the movements introduced by the US forcing within a volume $(\ell^*)^3$ are correlated and fall quite within one acoustic wavelength, and the corresponding phase increments picked up by light in that volume do not add up to a zero in the mean. The mean, $\langle\Delta\phi\rangle_{av}$ obtained from $g_1(\tau)$ (along with M) enriches the UMOT data enabling recovery of additional parameters such as refractive index, n, and the scattering coefficient, μ_s. For $\langle\Delta\phi\rangle_{av}$ to be nonzero, in addition to demanding that $\lambda_a >> \ell^*$, we should have a small enough ROI so that the intercept length of photon trajectory with the insonified ROI should have a good chance of being within ℓ^*. For this, our experience has been that if the ROI (which is usually an elongated hyperboloid with a narrow waist region) is bounded by $4-5$ times $(\ell^*)^3$, $\langle\Delta\phi\rangle_{av}$ will have a consistent nonzero value. In addition, we have shown in Sec. 2 that the length scale involved in phase decorrelation is $\ell_n^* = \ell_s(1 - \langle\cos\frac{\theta}{2}\rangle)$ which is larger than ℓ^*.

Our aim in this work is to demonstrate by simulations and experiments that $\langle\Delta\phi\rangle_{av}$ measured from the speckle modulation can be nonzero if the above mentioned conditions are met. A brief summary of the rest of the paper is as follows: In Sec. 2 we put forth an expression for $\Delta\phi$ in terms of displacements of scattering centers and the local n. Here we also discuss in detail the conditions under which $\langle\Delta\phi\rangle_{av}$ is nonzero. Sec. 3 discusses the details of our simulation studies. Here we vary the volume of the ROI and λ_a (in effect the US frequency), and obtain histograms of $\langle\Delta\phi\rangle$ measured at 256×256 elements in the CCD detector array. These histograms reveal a nonzero mean for $\langle\Delta\phi\rangle$ when λ_a is large and the US frequency is in the neighborhood of a dominant natural frequency of vibration of the ROI, and the ROI volume is small. Sec. 4 describes an UMOT experiment wherein poly-Vinyl Alcohol (PVA) phantoms and chicken breast-tissue slabs are used as samples. From the histograms obtained (from the measured $\langle\Delta\phi\rangle$ in all the elements in the detector array) we obtain $\langle\Delta\phi\rangle_{av}$ and demonstrate the sensitivity of the measured $\langle\Delta\phi\rangle_{av}$ to the local n in the ROI. Our concluding remarks are left to the last section (Sec. 5).

2. Theoretical considerations

Let N_p be the number of scattering events experienced by photons in their passage through the insonified ROI. The scattering centers are themselves vibrating because of sinusoidal US forcing. The typical displacement of the jth scattering center about its mean position is given by

$$\Delta\mathbf{r}_j(t) = \mathbf{u}(\mathbf{r}_j)\sin(\mathbf{k}_a.\mathbf{r}_j - \omega_a t). \tag{1}$$

Here $\mathbf{u}(\mathbf{r}_j)$ is the maximum displacement suffered by the jth scattering center, $\mathbf{k}_a$ is the acoustic wave vector, $\mathbf{r}_j$ is the position vector (at rest) of the jth scattering center and ω_a is the acoustic frequency. Fig. 1 shows a typical representation of scattering of light by a vibrating scattering center, with unit vectors in the incident and scattered photon directions (in a typical scattering event) represented by $\hat{k}_i$ and $\hat{k}_s$ ($\mathbf{k}_i$ and $\mathbf{k}_s$ are the corresponding wave vectors) and the displacement by $\mathbf{u}$ (taken as along $\hat{k}_i$ as shown in Fig. 1). The phase fluctuation experienced by the

photon following path p is given by [5]

$$\delta\phi_p(t) = \sum_{j=1}^{N_p} \mathbf{q}_j.\Delta\mathbf{r}_j(t). \tag{2}$$

Here $\mathbf{q}_j = \mathbf{k}_s - \mathbf{k}_i$. Since we consider electric field arriving along the same photon path alone to be correlated, the phase of the field autocorrelation of light reaching the detector along path p will have value:

$$\langle\Delta\phi_p(\tau)\rangle = \langle\delta\phi_p(t+\tau) - \delta\phi_p(t)\rangle \equiv \lim_{T\to\infty}\frac{1}{T}\int_0^T (\delta\phi_p(t+\tau) - \delta\phi_p(t))\,\mathrm{d}t. \tag{3}$$

To find the average $\langle\Delta\phi(\tau)\rangle_{av}$ which influences $g_1(\tau)$ we take the average of $\langle\Delta\phi_p(\tau)\rangle$'s evaluated over all the photon paths reaching the detector which have nonzero intercepts with the ROI, weighted by the probability density for the photon paths:

$$\langle\Delta\phi(\tau)\rangle_{av} = \int_{s_1}^{s_2} p(s)\langle\Delta\phi_p(\tau)\rangle\mathrm{d}s. \tag{4}$$

Here s is the photon path length, and s_1 and s_2 are limits on path lengths s which pertain to those with nonzero intercepts with the ROI. The integral in Eq. 4 can also be evaluated, un-
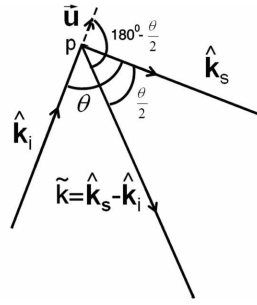

Fig. 1. Representation of a single scattering event from a point which suffered a maximum displacement of $\vec{u}$.

der weak scattering approximation, by first summing over $\langle\Delta\phi(\tau)\rangle$'s pertaining to all paths passing through a particular scattering center and then summing the result over all the scattering centers in the ROI [5]. When this is done $\langle\Delta\phi(\tau)\rangle_{av}$ can be nonzero only when there is scattering anisotropy for the medium to such an extent that $(\ell^*)^3$ is large enough to have the intercept length of the photon trajectory with the ROI $\leq \ell^*$. Moreover, while considering correlation of $\Delta\phi(\tau)$ one should use a scattering anisotropy factor $g_n = \langle\cos\frac{\theta}{2}\rangle$ to compute ℓ^* instead of the usual $g = \langle\cos\theta\rangle$. This results in a larger ℓ^* (denote it by ℓ_n^*) with which we can put limits on the volume of ROI so that $\langle\Delta\phi(\tau)\rangle_{av}$ is nonzero (as demonstrated in Sec. 3). (This can be seen from the diagram of Fig. 1. The phase, $\Delta\phi$ picked-up in a typical scattering event is $k_0\left(\hat{k}_s - \hat{k}_i\right).\mathbf{u} := k_0\tilde{k}.\mathbf{u} = k_0|\tilde{k}||\mathbf{u}|\cos\left(\pi - \frac{\theta}{2}\right)$, where k_0 is the modulus of light propagation vector. Therefore the uncertainty in $\cos\frac{\theta}{2}$, and not $\cos\theta$, determines the decorrelation of the overall phase fluctuation; and we use a modified $g_n = \langle\cos\frac{\theta}{2}\rangle$ as the anisotropy factor to arrive at ℓ_n^*). As we demonstrate through simulations, $\langle\Delta\phi(\tau)\rangle_{av}$ remains nonzero so long as the US focal volume V is bounded by $4 - 5$ times $(\ell_n^*)^3$. The reason for this persistence of correlation in $\langle\Delta\phi(\tau)\rangle_{av}$ over a larger volume compared to $(\ell_n^*)^3$ is that for the rather elongated shape of the ROI, the probability of a number of the intercept length of the photon trajectory with the ROI

remaining within ℓ_n^* is large for ROI volumes considerably larger than $(\ell_n^*)^3$. However, in our simulations we have used a cuboid ROI which is not elongated along any particular direction. The consequence of using this 'symmetric' object is that $\langle \Delta\phi(\tau) \rangle_{av}$ decays rapidly to zero as V increases from $(\ell_n^*)^3$ to $\sim 5(\ell_n^*)^3$ (See Fig. 2). In addition to the above there should also be
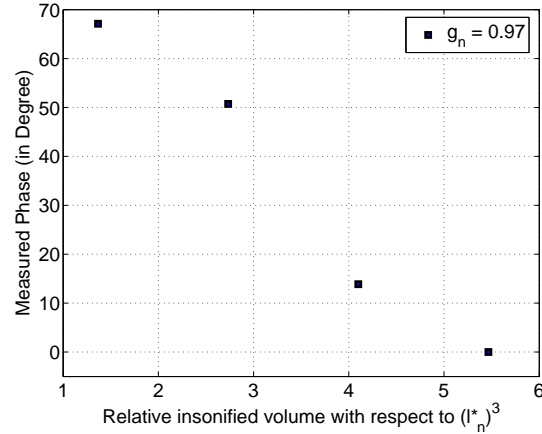

Fig. 2. Variation of $\langle \Delta\phi(\tau) \rangle_{av}$ (arrived at through MC simulation) with the volume of the ROI. Beyond $V = 4(\ell_n^*)^3$, $\langle \Delta\phi(\tau) \rangle_{av}$ fluctuates rendering the average not reliable.

'consonance' (i.e., directional bias along the US forcing) of the movement of scattering centers in the insonified region introduced by the ultrasound forcing, for $\langle \Delta\phi(\tau) \rangle_{av}$ to be nonzero. If $\lambda_a << \ell_n^*$, there will be many 'periods' of US-induced oscillations within the insonified volume, which would mean that the resulting oscillations (or displacements) of the scattering centers will have equal propensity to be in a certain direction and its opposite. Therefore for 'consonance' of the movement of scattering centers one should have $\lambda_a >> \ell_n^*$. This, however, is not enough to ensure that the movements will have correlatedness in direction (and not randomly distributed) so that phase picked up is not averaged to zero. The jelly-like material, which is the model used to represent tissue, for the particular shape of the insonified volume, has natural frequencies of vibrations in the range of $100 - 400\ Hz$ [6] corresponding to the axial translational mode. When the ultrasound forcing is at the natural frequency of vibration a resonance is observed in the oscillating movement of particles in the volume. In the vicinity of this resonant frequency, primarily only the prominent axial mode is excited (which sets up vibration along the US transducer axis) and the eigen values corresponding to the other modes such as non-axial translation, dilatation etc. are small. However when the forcing frequency is away from the resonant frequency of vibration, the input energy is more evenly distributed amongst all possible degrees of freedom with the result that oscillation amplitudes are more randomly oriented. Therefore when the forcing is at $1 - 2\ kHz$, even though one wavelength ($\sim m$) generously covers the insonified region, owing to the apparent randomness of the apparent displacements the average phase picked-up is seen to be zero.

Therefore, for the average phase to be nonzero we should have $V \sim 4 - 5$ times $(\ell_n^*)^3$ and $\lambda_a >> \ell_n^*$ (for typical soft biological tissue, $\ell^* \sim 1.00\ mm$ and $\ell_s \sim 0.10\ mm$ [7]), with the corresponding frequency close to the dominant natural frequency of vibration of the insonified region. In our experience (see Sec. 3) when the US frequency is below $1\ kHz$, i.e., $\lambda_a \sim 1.5\ m$, $\langle \Delta\phi(\tau) \rangle_{av}$ evaluated over a cuboidal ROI of volume $3 \times 7 \times 3\ mm^3 = 0.063\ cm^3$ is nonzero when $g_n \sim 0.97$ and $\ell_n^* = 3.58\ mm$. If we take $V = 5(\ell_n^*)^3$ this works out to be $5 \times 0.0461\ cm^3 = 0.2305\ cm^3$, much larger compared to the volume of the ROI.

Using Eqs 3 and 4 one can obtain computable expressions for $\langle \Delta\phi(\tau) \rangle_{av}$ in which the optical properties of the ROI and its size enter as parameters. In Sec. 3 we demonstrate through Monte Carlo (MC) simulations how $\langle \Delta\phi(\tau) \rangle_{av}$ varies when (i) $\frac{V}{(\ell_n^*)^3}$ is varied and (ii) $\Delta\nu$ the US forcing frequency is varied. We also demonstrate variation of $\langle \Delta\phi(\tau) \rangle_{av}$ when n is varied in the neighborhood of the ROI.
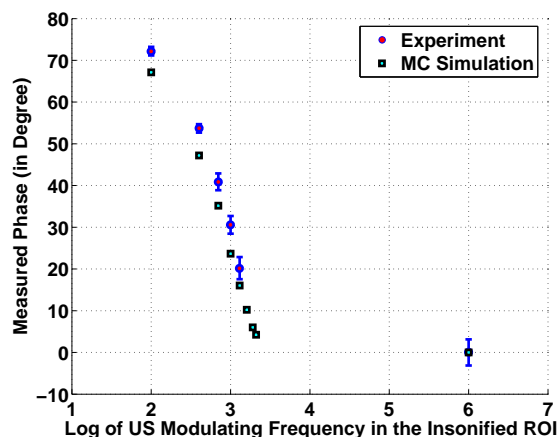
Fig. 3. Variation of $\langle \Delta\phi(\tau) \rangle_{av}$ with the ultrasound beat frequency. Beyond 1 kHz the variation in the mean is large and the measurement is inaccurate. The error in the experimental measurements is in the range of $4 - 6\%$.

3. Numerical simulations

For numerical simulations we consider a cylindrical object of diameter 3 cm and height 5 cm (to represent PVA phantom), and a slab $3 \times 3 \times 5$ cm^3 (to represent chicken breast sample). For PVA phantom, the optical properties used in the simulations are $\mu_a = 2.85 \times 10^{-4}$ mm^{-1}, $\mu_s = 10.00$ mm^{-1}, $g = 0.89$, and $n = 1.35$ [8], which is also varied to demonstrate the shift of $\langle \Delta\phi(\tau) \rangle_{av}$. For chicken breast tissue (slab of dimension $3 \times 3 \times 5$ cm^3) μ_a, μ_s and g are assumed to be 0.01 mm^{-1}, 23 mm^{-1} and 0.90 respectively in accordance with the properties of chicken breast tissue measured and reported in [9]. We use two identical focusing US transducers with focal regions intercepting in the object giving the ROI (for details, please see Section 4). The US focal volume of the individual transducer is assumed nearly hyperboloidal with axial length of ~ 1.2 cm and diameter across the waist (the thinnest middle region) 0.25 cm. The intersection of two such focal volumes which is labeled the ROI is assumed to be a cuboid of volume V. In fixing these parameters we took recourse to computing the acoustic pressure (by solving the Westervelt equation as is done in [10]) inside the focal volume of the hemispherical PZT transducers that we, in fact, employed in the experiments. The US focal volume is fixed as the region where the pressure is greater than 100th of its maximum pressure along the axis. The insonified volume, V, is varied in the simulations to demonstrate the dependence of $\langle \Delta\phi(\tau) \rangle_{av}$ on it.

First we carried out two sets of simulations to demonstrate the effect of $\frac{V}{(\ell_n^*)^3}$ and $\Delta\nu$ on $\langle \Delta\phi(\tau) \rangle_{av}$. In the first, through MC simulation, we compute the set of $\langle \Delta\phi(\tau) \rangle_{av}$'s from which histograms of $\langle \Delta\phi(\tau) \rangle_{av}$ are plotted for V going from $\sim 1.5(\ell_n^*)^3$ to $\sim 6(\ell_n^*)^3$. The results plotted in Fig. 2 show that the mean obtained from the histogram steadily goes to zero as V is increased from $\sim 1.5(\ell_n^*)^3$ to $\sim 6(\ell_n^*)^3$.
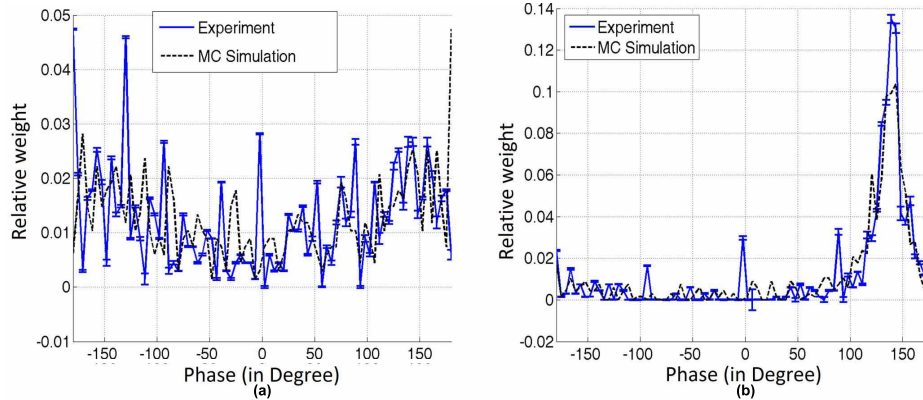
Fig. 4. Histogram of the phase fluctuation obtained from experiments and simulations. The object used is the PVA phantom. When the US frequency is (a) $1\ MHz$ the mean is close to zero; when it is (b) $100\ Hz$ the histogram has a clear bias with a peak around $140°$ (for experiment) and $145°$ (for simulations). The percentage error in phase extracted through measurements is $1-6\%$ depending on intensity level.

In the second set of simulations we varied $\Delta \nu$ from $100\ Hz$ to $2\ kHz$ in the steps of $250\ Hz$ and computed $\langle \Delta \phi(\tau) \rangle_{av}$. For $\Delta \nu > 1\ kHz$ the average phase is close to zero, verified also for a high frequency of $1\ MHz$. Here, the dimensions of the ROI is kept at $3 \times 7 \times 3\ mm^3$ and the other optical properties are kept at values same as those used in the first set. The plot of the $\langle \Delta \phi(\tau) \rangle_{av}$ .vs. $\Delta \nu$ obtained through simulations is shown in Fig. 3, which also shows results from the experiments described later in Sec. 4.
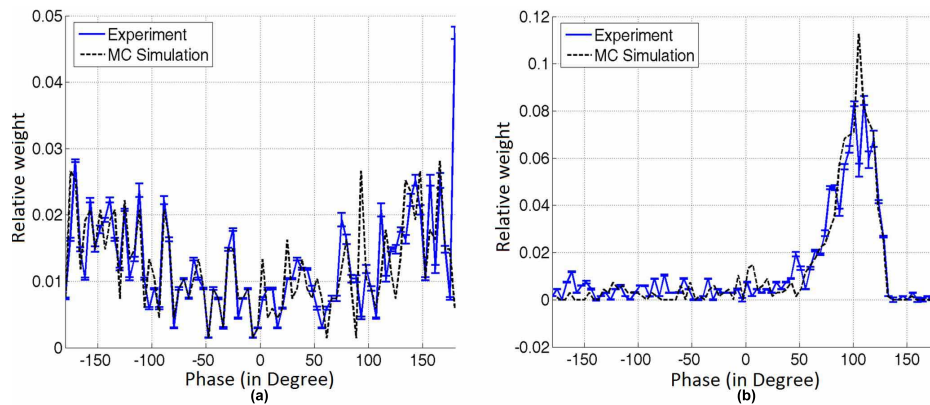

Fig. 5. Histogram of the measured phase fluctuation obtained from experiments and simulations. The object used is a slab of chicken breast which contains water in the ROI. When the US frequency is $1\ MHz$ the phase fluctuation is random with the mean close to zero (a) and when it is $100\ Hz$ the histogram has a clear bias with a peak around $110°$ (for experiment) and $105°$ (for simulations) (b). The percentage error in phase extracted through measurements is $1-8\%$.

For arriving at $\langle \Delta \phi(\tau) \rangle_{av}$ we proceeded as follows: 5×10^7 photons are propagated using Monte Carlo simulation to compute the photon path distribution in the object in the transmission geometry. We kept track of, primarily, the optical path length of photons in the insonified ROI and the photon weight from which the distribution of photon phase fluctuation is found,

using Eqs 3 and 4 at various exit points corresponding to the 256×256 elements in the CCD camera. (The details of MC simulation used are given in [11, 12]). From this we have plotted histograms of $\langle \Delta\phi(\tau) \rangle_{av}$ for two US beat frequencies of $\Delta v = 1\ MHz$ and $100\ Hz$. These are shown in Fig. 4(a) and (b) respectively for the cylindrical PVA phantom described earlier with n around the ROI assumed to be 1.33. Histograms obtained from experimentally generated phase distribution (details in Sec. 4) are also shown in the figure for comparison. When we repeated the simulations for the slab of chicken breast (with water, $n = 1.33$) in the ROI the histograms shown in Fig. 5(a) and 5(b) are obtained for $\Delta v = 1\ MHz$ and $100\ Hz$ respectively. It is seen that when frequency is $100\ Hz$ the evaluated average phase in the two cases are $145°$ (for PVA) and $105°$ (chicken breast). When the simulation is repeated for chicken breast slab with glycerol in the ROI ($n = 1.47$) with frequency of $100\ Hz$ we obtained the histogram shown in Fig. 6 with $\langle \Delta\phi(\tau) \rangle_{av}$ extracted as $120°$. It is seen that the average phase fluctuation shifts when the n in the ROI changes. As stated earlier the above set of figures come with corresponding experimental results overlaid which will be explained in the next section.
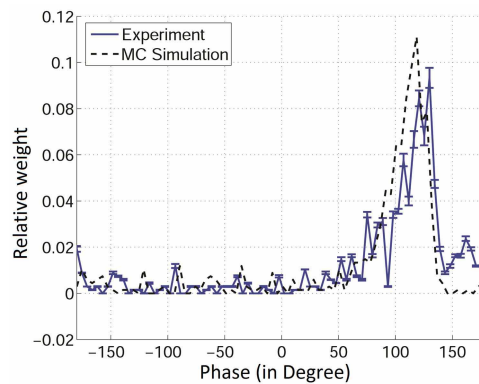

Fig. 6. Same as 5(b) but with glycerol injected around the ROI. It is seen that owing to the higher n of glycerol the average phase has increased to $\approx 130°$ (for experiment) and $120°$ (for simulations). The percentage error in phase extracted through measurements is $1 - 7\%$.

4.   Experiments

Our experimental set-up is similar to the one introduced in [13, 14] for UMOT which uses a source-locking technique to measure speckle modulation (of frequency as high as $1\ MHz$) with a slow $50 - 60\ Hz$ CCD camera. For more details see [11]. It adapts the 4- or 3- intensity method of phase shift interferometry to compute the modulation and phase of interference patterns by recording 4 frames of intensities with preset phase differences between reference and object beams [15]. The system essentially uses a modulated laser beam locked to the driving oscillator of the US transducer. A low frequency acoustic excitation in the range of $100\ Hz$ to $1\ kHz$ is required to obtain the resonance of vibrating ROI of jelly-like soft tissue-mimicking phantom [6] while US frequency of the order of MHz is demanded to achieve penetration depth of the order of $cm's$ in soft tissue. Here, we employed two identical, focusing US transducers (Panametrics, V394-SU-F50MM-PTF) operated in continuous mode with a small and adjustable frequency difference; one at $v_1 = 1\ MHz$ and the other at $v_2 = v_1 + \Delta v$ (with the possibility of Δv to be fixed accurately in the range $100 - 1200\ Hz$). The transducers are aligned, with the angle of inclination $60°$ (at the depth $1.5\ cm$ inside the tissue samples), to have an intersecting common focal region and US induced low frequency acoustic wave at the beat frequency Δv at the region of intersection [11]. The experimental set-up is schematically shown in Fig. 7. During
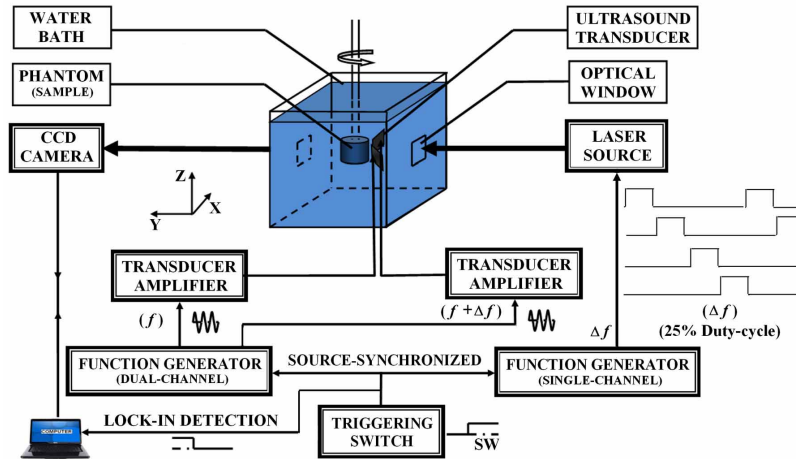
Fig. 7. Schematic diagram of the experimental set-up. The CCD camera is focused onto the optical window. For a fuller description of the parts shown see Ref. [11].

the experiments, the samples are immersed in water (as shown in Fig. 7) for proper acoustic impedance matching. For entry and exit of light there are optical windows provided in the container. ROI is the narrow region of intersection of the two focal regions as depicted in Fig. 8. The near infrared (NIR) laser beam (of diameter 2 mm) of wavelength 785 nm is used to interrogate the US insonified ROI sent along the direction bisecting the angle subtended by the two US beams and the transmitted US modulated optical signal is collected using a CCD camera (JAI, CV-M10 BX, 25 frames/sec) (see Fig. 8). The laser beam is intensity modulated whose injection current is a biased square wave of frequency Δv and duty cycle of 25% composed of $40 - mA$ off-state and $60 - mA$ on-state, with Δv equal to the US beat frequency. The laser diode is phase-locked to the function generator driving the US transducers and can be phase-shifted with respect to this latter drive signal. For a particular value of Δv Hz we recorded four sequential speckle intensities with the CCD camera (with an exposure time of 40 $msec$ each) each corresponding to phase shifts between the laser diode and US transducer drive signals of 0, $\frac{\pi}{2}$, π and $3\frac{\pi}{2}$ radians. From these four intensities $\Delta\phi$ is computed using the formula given in Eq. A5 of Ref. [11] for each of the pixels, resulting in an ensemble of $\Delta\phi$'s. From this ensemble we compute a histogram of the distribution of phase in the range $(-180°, 180°)$.

In the first set of experiments we have used a cylindrical PVA phantom of dimensions and optical properties as given in Sec. 3. Experiments are conducted at number of frequencies starting at 100 Hz going up to 1 MHz, and the $\Delta\phi$ histograms are computed. From the histogram $\langle\Delta\phi\rangle_{av}$ is computed and plotted against Δv in Fig. 3. For comparison, a similar plot obtained from numerical simulation is also shown. It is observed that the spread in the $\langle\Delta\phi\rangle_{av}$ values, in both the simulated and experimental results gets larger as the frequency increases. Beyond around 750 Hz, $\langle\Delta\phi\rangle_{av}$ becomes both smaller and spread around the mean (Fig. 3). The obtained average phase is erroneous and unreliable beyond, say, 1 kHz.

From the above experiment, the histogram obtained for two typical frequencies, namely, 1 MHz and 100 Hz are shown in Fig. 4(a) and Fig. 4(b) respectively. For 1 MHz, $\Delta\phi$ is uniformly distributed around $0°$ (without any bias towards any angle) indicating that $\langle\Delta\phi\rangle_{av} = 0$ (Fig. 4(a)), and for $\Delta v = 100$ Hz it is peaked around $140°$ (Fig. 4(b)). In Fig. 4, we overlaid the
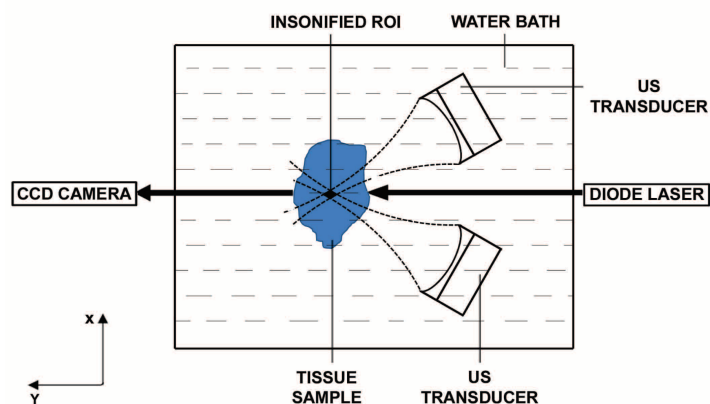
Fig. 8. Schematic diagram showing a typical cross section of the experimental set-up. Two focusing ultrasonic waves from the transducers are intersecting each other inside the tissue subtending an angle of $60°$. A narrow laser beam (of diameter $2\ mm$) is incident onto the sample along the direction bisecting the subtending angle of the US focusing waves and the CCD faces the diode laser as shown to collect the transmitted light.

corresponding simulated histograms obtained from Sec. 3 for comparison; and the match between the simulated and experimental histograms and the averages is seen to be very good. This clearly demonstrates that the phase fluctuation has a nonzero mean when λ_a becomes very large compared to ℓ_n^* and the corresponding frequency is close to a natural frequency of vibration of the ROI.

Similar histograms obtained by repeating the above experiment in the chicken breast slabs (with water, $n = 1.33$, in the ROI) are shown in Fig. 5(a) and Fig. 5(b) for $1\ MHz$ and $100\ Hz$ respectively. The average phase extracted from the low frequency histogram is seen to be $110°$.

In the next experiment we use an almost dry chicken breast slab with glycerol ($n = 1.47$) injected (using a hyperdermic syringe) so that the ROI is awash with glycerol. The new histograms (experimental as well as simulated) are shown in Fig. 6. It is seen that the $\langle \Delta\phi \rangle_{av}$ here is shifted to $130°$ for glycerol with $n = 1.47$ when compared to the first experiment for which the sample which is supposed to have water in the background with $n = 1.33$ gave the corresponding value as $110°$. This clearly brings forth the role $\langle \Delta\phi \rangle_{av}$ can play in detecting changes in n deep within biological tissue samples.

5. Conclusions

In this study we demonstrate through simulations and experiments that the phase fluctuations carried by light propagating through the US focal volume can have a nonzero mean. Working under weak scattering approximation, the first condition to be met for the above mean to be nonzero is that the material should have a large g such that the US focal volume is bounded by $4 - 5$ times $(\ell_n^*)^3$. Another important requirement is that the phase picked-up by light scattering events within the ROI should not be averaged out by the randomness of the oscillations induced by the US forcing. For this it is not enough that $\lambda_a >> \ell_n^*$ but also the frequency corresponding to the λ_a employed should be in the vicinity of the dominant natural mode of vibration of the insonified ROI. The nonzero mean of the phase of the ultrasound modulated light is an extra measurement that can be used to recover refractive index change in a localized region in the tissue specified by the US focal position. If in addition to the modulation depth M, phase is also

available through an UMOT experiment, albeit an average one, this can be used to construct an artificial hologram. This, in turn, can be used to recover a conjugate wave to back-propagate to the ROI forming either a μ_a- or shear modulus image of the ROI. These can be the subjects of future investigations.